

Secular spring rainfall variability at local scale over Ethiopia: trend and associated dynamics

Gizaw Mengistu Tsidu^{1,2,3} 

Received: 17 September 2014 / Accepted: 17 June 2016 / Published online: 16 July 2016
© Springer-Verlag Wien 2016

Abstract Spring rainfall secular variability is studied using observations, reanalysis, and model simulations. The joint coherent spatio-temporal secular variability of gridded monthly gauge rainfall over Ethiopia, ERA-Interim atmospheric variables and sea surface temperature (SST) from Hadley Centre Sea Ice and SST (HadISST) data set is extracted using multi-taper method singular value decomposition (MTM-SVD). The contemporaneous associations are further examined using partial Granger causality to determine presence of causal linkage between any of the climate variables. This analysis reveals that only the northwestern Indian Ocean secular SST anomaly has direct causal links with spring rainfall over Ethiopia and mean sea level pressure (MSLP) over Africa in spite of the strong secular covariance of spring rainfall, SST in parts of subtropical Pacific, Atlantic, Indian Ocean and MSLP. High secular rainfall variance and statistically significant linear trend show consistently that there is a massive decline in spring rain over southern Ethiopia. This happened concurrently with significant buildup of MSLP over East Africa, northeastern Africa including parts of the Arabian Peninsula, some parts of central Africa and SST warming over all

ocean basins with the exception of the ENSO regions. The east-west pressure gradient in response to the Indian Ocean warming led to secular southeasterly winds over the Arabian Sea, easterly over central Africa and equatorial Atlantic. These flows weakened climatological northeasterly flow over the Arabian Sea and southwesterly flow over equatorial Atlantic and Congo basins which supply moisture into the eastern Africa regions in spring. The secular divergent flow at low level is concurrent with upper level convergence due to the easterly secular anomalous flow. The mechanisms through which the northwestern Indian Ocean secular SST anomaly modulates rainfall are further explored in the context of East Africa using a simplified atmospheric general circulation model (AGCM) coupled to mixed-layer oceanic model. The rainfall anomaly (with respect to control simulation), forced by the northwestern Indian Ocean secular SST anomaly and averaged over the 30-year period, exhibits prevalence of dry conditions over East and equatorial Africa in agreement with observation. The atmospheric response to secular SST warming anomaly led to divergent flow at low levels and subsidence at the upper troposphere over regions north of 5° S on the continent and vice versa over the Indian Ocean. This surface diffluence over East Africa, in addition to its role in suppressing convective activity, deprives the region of moisture supply from the Indian Ocean as well as the Atlantic and Congo basins.

✉ Gizaw Mengistu Tsidu
gizaw_mengistu@gmx.net

¹ Department of Earth and Environmental Sciences, Botswana International University of Science and Technology, Priv. Bag 16, Palapye, Botswana

² Department of Physics, Addis Ababa University, P.O. Box 1176, Addis Ababa, Ethiopia

³ Karlsruhe Institute of Technology (KIT), Institute of Meteorology and Climate Research, 76344 Leopoldshafen, Karlsruhe, Germany

1 Introduction

The major impacts of climate change are related to temperature and rainfall. The changes in rainfall patterns are the strongest felt since the changes may lead to floods or droughts in different areas. Moreover, rainfall is a decisive element in agriculture. In this regard, the impacts of

rainfall variability at various temporal scales on regions such as sub-Saharan Africa where rainfed agriculture serves as the main lifeline for both food security and national economy are immense. Rainfall is also considered as the primary source of water in the region. Thus, most water resource-related development projects should take information on historical pattern of rainfall variability into account during the planning phase. Moreover, rainfall is one of the most potent variables in diagnosing climate change and providing signatures of eco-environmental response to climate change (Cannarozzo et al. 2006; Oguntunde et al. 2006; Guo et al. 2006).

As a result, a number of studies have been undertaken to understand the Sahel rainfall following the 1960s, 1970s, and 1980s droughts and the famine that followed (Lamb 1978a; Folland et al. 1986; Degefu 1987; Seleshi and Demaree 1995; Camberlin 1997; Gissila et al. 2004; Segele and Lamb 2005; Shanko and Camberlin 2005; Sylla et al. 2009; Diro et al. 2011). For example, Giannini et al. (2003) have shown that both low- and high-frequency characteristics of the observed Sahel drought can be reproduced by prescribing observed SSTs alone as a boundary condition for a global climate model. The authors concluded that the Indian Ocean plays greater role than the tropical Atlantic and Pacific in decadal-scale variability while high-frequency variability is dominated by the Pacific Ocean basin SST. A number of other simulations (Bader and Latif 2003; Lu 2009; Hagos and Cook 2008) have come to the same conclusion that the Indian Ocean SST plays the dominant role in the observed Sahel drought. On the other hand, a few other studies failed to show the causal link between the Indian Ocean SST and Sahel rainfall (Hoerling et al. 2006; Caminade and Terray 2010). For instance, Caminade and Terray (2010) argued that the interhemispheric SST asymmetry observed after 1970 is responsible for the Sahel drought. Obviously, the relationship between the Sahel rainfall variability and global ocean basins SST is widely studied though the main focus is on the West Africa monsoon/summer rainfall regions.

East Africa rains are equally important as monsoon-related rainfall account for major fraction of the annual total rainfall. As a result, a number of studies focused on East Africa spring and autumn rainfall variability have also been conducted (Habtemichael and Pedgley 1974; Ogallo 1989; Camberlin 1995; Nickolson 1996; Vizy and Cook 1998; Goddard 1999; Sun et al. 1999b; Mutai and Ward 2000; Camberlin and Philippon 2002a; Nicholson and Grist 2003; Schreck and Semazzi 2004; Slingo et al. 2005; Mwale and Gan 2005; Zhou et al. 2006; Hastenrath 2007; Hastenrath et al. 2010; Segele et al. 2008; Bahaga et al. 2014) to understand the rainfall characteristics, circulation mechanisms and links to remote SST forcing mostly at seasonal to interannual/interdecadal time scales.

Recently East Africa has experienced a number of disaster events due to changes in rainfall. The severe droughts of 2009, 2011, and 2015, and torrential rains that led to the floods of 2009 are events that occurred in recent times. The severity and increase in the frequency of the recent droughts over the region might be linked to climate change. However, unlike robust studies of East Africa, rainfall variability at seasonal to interannual/interdecadal time scales, both observational and model studies of the East Africa region at secular time scale are very few (Seleshi and Camberlin 2006; Seleshi and Zanke 2004; Jury 2009; Lyon and DeWitt 2012; Tierney et al. 2013) and are limited in scope either due to sparse data or absence of robust investigation on physical mechanisms. Notably, the mechanisms of rainfall variability in the region as driven by SST changes at the secular time scale are lacking. The rainfall characteristics over land is driven by both locally available and transported moisture (Brubaker et al. 1993; Trenberth et al. 2003; Mengistu Tsidu et al. 2015), and therefore, the local dynamical patterns of convergence or divergence are crucial. A full accounting of the role of these processes in rainfall variability require robust observations complemented by process studies using AGCM. Despite this necessity to understand the nature and causes of long-term changes, the volume of work done in this direction over the region is insufficient owing to either relatively short or sparse climate records which also suffer from inhomogeneity.

Since the problem of data availability and inhomogeneity is not unique to the region, some studies have been conducted to alleviate the problem through reconstruction of homogeneous climate variables from blended satellite and ground-based observations (e.g., rainfall estimates from satellites and rain gauge) or in situ ground-based observations (Xie and Arkin 1996, 1997; Adler et al. 2003, 2005; Mitchell and Jones 2012; Mengistu Tsidu 2012). The data sets are mostly interpolated to regular grids and are presented in the form of gridded data with various horizontal resolutions depending on the density of observations. For instance, one of the most recent data set developed as part of monitoring climate-related risks over Africa is the Climate Hazards Group Infrared Precipitation with Stations (CHIRPS) rainfall data (Funk et al. 2014). Recently, Mengistu Tsidu (2012) has developed a homogenized, quality-controlled, and gridded rainfall data set using pure gauge rainfall from relatively dense network of stations over Ethiopia with a horizontal resolution of 50 km. This work aims to take advantage of the improved availability and data quality from these studies over the region in order to understand secular rainfall variability.

The purpose of this paper is to extract long-term coherent spatio-temporal changes in spring rainfall (February to May (FMAM)) from the later data set over Ethiopia and

determine the atmospheric and oceanic signals that modulate secular rainfall variability. The paper assesses evidences of climate change signal over Ethiopia from the analysis of a 30-year gridded rainfall data spanning the 1978–2007 period. ERA-Interim atmospheric fields and SST from HadSST1 data set are employed to understand the underlying mechanisms that control secular rainfall variability. MTM-SVD is used to identify joint coherent secular variances of rainfall, MSLP, and SST over tropical ocean basins. Since MTM-SVD is able to indicate only joint variability, partial Granger causality analysis is used to identify the causal link between rainfall, MSLP over Africa, and SST. A simplified AGCM coupled to mixed-layer oceanic model, SPEEDY, is then employed to evaluate the plausible causal connection between spring rainfall over Ethiopia and variable(s) identified as having strong linkage with rainfall from Granger causality analysis. The AGCM experiments are used to ascertain mechanisms of forcing of secular rainfall anomalies by the identified agent(s) of forcing. The paper is organized such that description of the study area is given in Section 2. Section 3 describes the data set and the different methods used for the analysis where as Section 4 highlights the main features and improvement of the SPEEDY AGCM over time. Results and discussions are given in Section 5 and conclusions are presented in Section 6.

2 Description of the study area

Ethiopia lies in the tropics and its climate is characterized by high rainfall and temperature variability at both spatial and temporal scales. The variability in distribution is related with altitude, latitude, humidity, and winds which are the significant factors in affecting the weather system of the area. It has a complex topography varying from 4,500 m above sea level in the north and central regions to 100 m below sea level in the north-eastern part of the country. The major topographic feature of the country includes high plateau and mountain chains on either sides of the northeast-southwest-oriented great East African Rift Valley. These highlands serve as a buffer zone between the Rift Valley and the lowlands in the border regions with Sudan, Somalia, Kenya, and Djibouti. Because of these complex topographical and geographical features, the climate of Ethiopia exhibits strong spatial variations and different rainfall regimes (Slingo et al. 2005; Mengistu Tsidu 2012). For example, the eastern regions exhibit bimodal (two wet periods throughout the year) rainfall distributions in summer (June–September) and spring (February–May) while the southern regions show the bimodal rainfall pattern in spring and autumn (October–December).

3 Data and methodology

3.1 Data set

A rainfall data set, that undergone homogeneity test and adjustment using the RHtestsV3 software package (Wang et al. 2010), Multi-channel Singular Spectrum Analysis (MSSA) (Ghil and Taricco 1997; Ghil et al. 2002) for filling missing data and ordinary Kriging for creating a regular 0.5 degree spatial resolution, is used in this study. The quality of the gridded data set as well as the intercomparison with other independent data set is thoroughly discussed in our earlier paper (Mengistu Tsidu 2012).

Sea level pressure, geopotential height, zonal and meridional winds data from ECMWF ERA-Interim on a horizontal resolution of 0.75×0.75 degree and variable vertical resolution with a 6-hourly analysis frequency (Berrisford et al. 2009; Dee et al. 2011) are employed in the study. The SST data at a horizontal resolution of 1.0×1.0 degree are taken from the Met Office Marine Data Bank (MDB), which from 1982 onwards also includes data received through the Global Telecommunications System (GTS) (Rayner et al. 2003).

3.2 Methodologies

3.2.1 Multi-taper method singular value decomposition

Multi-taper method singular value decomposition (MTM-SVD) is used to identify frequency of coherent spatio-temporal covariabilities of rainfall, atmospheric, and oceanic fields. The method has been used to analyze joint spatio-temporal variability of climate drivers and climate signal (Mann and Park 1996a, b; Mann et al. 1995; Delworth and Mann 2000; Somkiat et al. 2009). Thus, the method can be used to study plausible mechanisms of joint variability of these variables. The extraction of anomalies with respect to long-term mean at a given time scale (frequency) using MTM-SVD has the advantage over many spectral methods that the extracted signal has the same spatial and temporal dimensions as the original data (Mann et al. 1995; Mann and Park 1996a, b; Delworth and Mann 2000; Somkiat et al. 2009; Correa-Ramirez and Morales 2012; Mengistu Tsidu and Ture 2013; Mengistu Tsidu et al. 2013).

The method identifies the frequencies that are statistically significant among a large number of normalized independent series (e.g., multiple grid points) in terms of contribution of a significant fraction of the total data variance. The normalized singular values from the first mode in MTM-SVD analysis are proportional to the variability on each sampling frequency and are used to build the power spectra of local fractional variance (LFV).

Data sets of rainfall over Ethiopia, mean sea level pressure (MSLP) over Africa and adjacent Oceanic Basins, and SST over tropics within $30^{\circ}S - 30^{\circ}N$ for MTM-SVD analysis are arranged on space-time matrix ($M \times N$) such that rainfall, MSLP and SST are defined at a total of 376 (0.5 degree resolution), 918 (3-degree resolution) and 4080 (2-degree resolution) grid points, respectively, contributing to a total of $M = 5374$ grid points and a temporal length of $N = 116$ time units (i.e a month) from 1979 to 2007 for the extended spring season consisting of 4 months (February, March, April, and May) per year. To ensure no interference from grid points with high variance during the MTM-SVD analysis, the data series in each matrix were standardized by removing the mean and standard deviation. The data series are also weighted by multiplying them with the cosine of their respective latitude and a weighting factor in order take the difference in area covered by grid points into account. The time step is $\frac{1}{4}$ year in order to have a unique time series covering the above period of study.

3.2.2 Partial Granger causality analysis

The joint coherent variabilities between climate variables identified from the MTM-SVD analysis cannot indicate directional couplings (causal linkage) alone. The large contemporaneous correlation from such analysis could also be due to common external influences. Therefore, the causality between climate variables in the Granger sense (Granger 1969) should complement MTM-SVD analysis in order to assess causality. The concept of Granger causality, a statistical understanding of causality, is originally used in econometrics (Granger 1969). The method has since evolved to encompass widespread applications in many fields (Elsner 2007; Smirnov and Mokhov 2009, 2015) and is usually implemented via autoregressive modeling of multivariate time series. The basic idea is based on the assumption that the cause temporally precedes the effect, and the embedded information in the cause about the effect is unique enough (Granger 1969) to predict the effect.

When analysis of causality for multivariate is sought, a simple approach is to apply it to all possible pairs of signals since Granger causality is defined for only two time series traditionally. However, an indirect relationship can lead to spurious causal links. Conditional Granger causality is developed to overcome this problem and works by explicitly removing the influence of a third signal. The conditional Granger causality can handle indirect links provided that all relevant variables are included in the multivariate analysis. The presence of all relevant variables cannot be ensured most of the times since unmeasured latent variables can confound real causal influences. Partial Granger causality is an extension of conditional Granger causality and can deal with the issue of external and latent variables.

In this study, the partial Granger causality is employed to a multivariable time series composed of secular spring rainfall over Ethiopia, MSLP over Africa, spatially averaged SSTs over the northwestern India Ocean, southern Indian Ocean, equatorial Atlantic Ocean, northern Pacific Ocean and southern Pacific Ocean basins. The area which is included in the spatial averaging is selected because the areas are identified from MTM-SVD analysis as having strong joint covariances of SST and MSLP with spring Ethiopian rainfall.

3.2.3 Mann Kendall trend test and Prewhitening

The secular anomaly time series reconstructed from MTM-SVD analysis at $f = 0 \text{ cycles} \cdot \text{year}^{-1}$ could be either a trend or long-term periodic changes with the period exceeding half of the length of the time series. The linear trend detection was carried out for this signal for each grid point over Ethiopia using the Mann-Kendall (MK) test (Mann 1997; Kendall 1975). The MK test, non-parametric and rank-based procedure, has been widely used to test for randomness against trend in climatology and hydrology (Mann 1997; Kendall 1975) since it is robust and very reliable for extreme and skewed variables such as rainfall.

The MK test requires time series to be without serial correlation. Prewhitening, as described by Kumar et al. (2009), of the dataset before applying the MK test is advised (Abdul Aziz and Burn 2006; Jhahharia et al. 2011; Dinpashoh et al. 2011) to minimize or to eliminate significant positive serial correlation which influences the MK test.

4 Diagnosis of observed circulation using AGCM model experiments

The SPEEDY AGCM is used to diagnose the circulation mechanisms inferred from MTM-SVD of rainfall, SST and atmospheric fields. The SPEEDY AGCM model developed at International Centre for Theoretical Physics (ICTP) (Molten 2003) is applied for this purpose. The model, which has been improved substantially over time (Bracco et al. 2004; 2007), is based on a hydrostatic spectral dynamical core and uses the vorticity divergence form described by Bourke (1974). The model has been used in several studies (Kucharski et al. 2006a, b, 2007). The model is configured with a spectral truncation at a total of 30 wavenumbers and eight vertical sigma levels for this investigation. Five sets of experiments are performed. The AGCM is forced by observed SSTs anomalies in the first experiment to assess the performance of the model in reproducing the observed climatologies over the region. The AGCM is forced by climatological SST in second experiment, called control run hereafter. A third experiment, which is referred

to as the sensitivity experiment hereafter, is also forced by climatological SST except over northeastern Indian Ocean basin where the secular SST anomaly, extracted from MTM-SVD multitaper spectral method, is superimposed on the climatological SST. The northwestern Indian Ocean refers to basin that encompass areas between latitude of 15°S and 30°N and longitude of 37°E and 75°E. The atmosphere is coupled to the Ocean through the mixed layer oceanic model in all of the above simulations. Additional two sets of control and sensitivity experiments were conducted with no coupling of the atmosphere to the Ocean. This is to assess whether atmospheric forcing of the Ocean through SST feedbacks has impact on the secular rainfall variability or prescribed secular SST anomalies alone can force observed secular spring rainfall anomaly over Ethiopia. Since SPEEDY is a simplified model, the objective here is not to reproduce the observed secular rainfall anomalies in response to prescribed secular SST anomalies over northeastern Indian Ocean. Instead, the target here is to find out whether the model simulation captures the observed direction of the anomalies in the rainfall and circulation patterns.

5 Results and discussions

5.1 Joint secular variance

Figure 1 shows the LfV spectra for the joint variation of monthly rainfall, regional MSLP and tropical SST for spring time series. The time series are first deseasonalized after removing long term monthly mean and then are subjected to standardization by the variance and MTM-SVD analysis sequentially. The prominent signal is the secular component for the monthly time series. The annual signals is another prominent signal. There are also some interannual signals that are significant at least at 90 % significance level.

Figure 2a shows percentage of total variance explained by the secular component of the rainfall extracted from monthly time series of FMAM rainfall over a period from

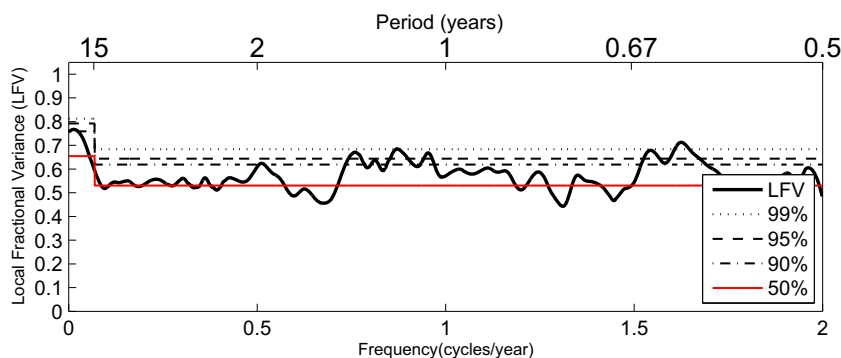
1979 to 2007. The rainfall variance explained by the secular component (Fig. 2a) is maximum and exceeds 50 % at few isolated locations over southwestern and southeastern highlands of the country, remains in the range of 20–30 % over southeastern low and highlands located between 40–43°E and western lowlands. The secular spring rainfall variance northward of 9°N has less significance since the contribution of spring rainfall to the annual total rainfall is either none or negligible.

The secular FMAM MSLP variance (Fig. 2b) is maximum (i.e., in excess of 60 % of the total variance) over central Africa regions. The secular MSLP variance accounted for 30–50 % over whole of southern Africa, southwestern Ethiopia and parts of western Africa. Secular MSLP variance exceeding 15 % of the total variance is also observed over the St. Helena high pressure system and Arabian Peninsula. The secular SST variance (Fig. 2c) represents dominant fraction of the total variance over the equatorial Atlantic (in excess of 50 % over mainly north of equator), northern Indian Ocean (20–30 %) and Pacific Ocean outside ENSO regions (30–50 %). The significant contribution of the secular variance to the total joint variance of Ethiopian spring rainfall, SST and MSLP implies presence of strong statistical associations between the climate variables.

5.2 Linear trend in the secular rainfall signal

The secular varying component of the rainfall over Ethiopia is a slowly varying signal as a function of time which may not be necessarily linear. This means that a linear trend can be estimated through fitting linear function to the anomaly time series or by means of procedures described under Section 3.2.3. Here, we have estimated the linear trends using the latter procedure. The statistical significances of the estimated trends are tested using Mann-Kendall’s trend significant test with the levels of significance at 0.01 ($z_{\frac{\alpha}{2}} = \pm 2.58$) and 0.05 ($z_{\frac{\alpha}{2}} = \pm 1.96$). Figure 3a shows the linear trend of spring rainfall over Ethiopia in units of $mm.decade^{-1}$. The prominent feature is the steep rate of decline in rainfall in the last 30 years (up to 28

Fig. 1 The LfV spectra of coherent covariation of gridded Ethiopian rainfall, ERA-Interim MSLP and tropical SST from HadISST dataset for FMAM season using MTM-SVD procedure



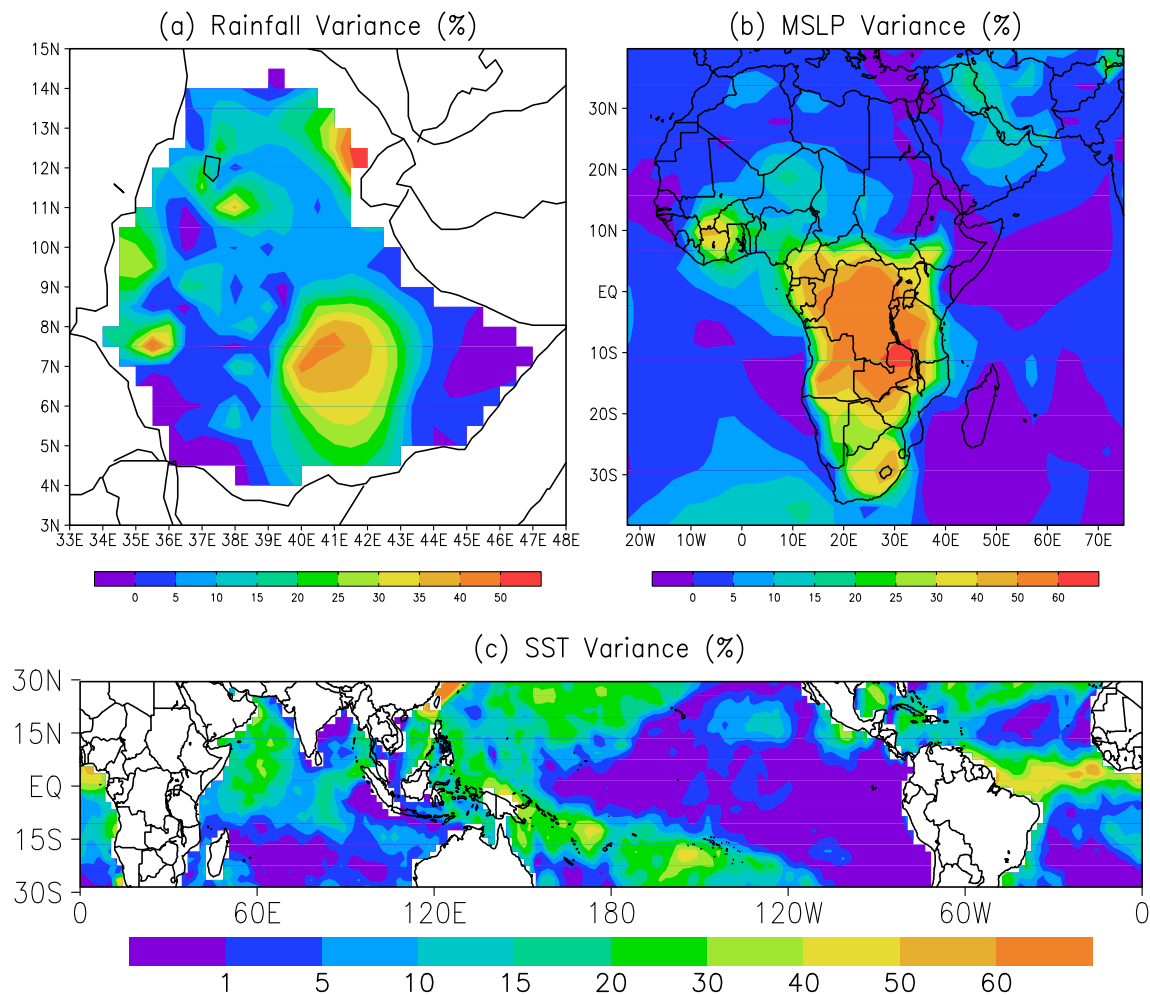


Fig. 2 Rainfall (a), MSLP (b), and SST (c) variances contributing to the secular variation at $f = 0$ cycles per year shown in Fig. 1 during extended spring (FMAM) season

$mm.decade^{-1}$) over the southern and adjoining eastern highlands. The spatial distribution of z -scores determined from the Mann-Kandall trend test (not shown) indicates that all trend values are significant at 99 %.

The trend in MSLP shows pressure buildup over most part of continental Africa and parts of western Indian Ocean while Western Africa and Asia experience negative trend creating east-west pressure gradients (Fig. 3b). Concurrently, the SST shows warming trend over all ocean basins with the exception of the northern Pacific and a small pocket of the southern Atlantic basin near St. Helena high pressure which exhibit cooling trend, as well as the ENSO regions of the Pacific and southern Indian Ocean which remain near normal (Fig. 3c).

The coherence of the phase of secular SST anomalies (not shown) and trend in secular SST anomalies over western Pacific warm pool with SSTs in the eastern Indian Ocean (Fig. 3) is consistent with the known influence of the Indonesian Throughflow on the southeastern Indian Ocean SST. Moreover, Tierney et al. (2013) have

compared a recent sedimentary reconstruction of SST from the Makassar strait for the western Pacific warm pool over the past millennium (Oppo et al. 2009), assuming the known influence of the Indonesian Throughflow on the southeastern Indian Ocean SST with lacustrine hydroclimatic proxy records from East Africa and found a remarkable similarity between the temporal evolution of Makassar SST and East African climate. These palaeoclimate data support the mechanistic link between the eastern Indian Ocean SST and East African rainfall seen in the AOGCM control runs by Tierney et al. (2013), wherein cool SST in the eastern Indian Ocean is associated with wet conditions along the East African coast. This mechanistic link is also evidently present in this study from association of warm secular SST anomalies over the Indian Ocean and dry conditions over southern Ethiopia during FMAM.

The observed phase coherence between rainfall, MSLP, and SST at secular time scale may not necessarily imply causal links between the variables in the case of presence of a common unaccounted external influence. The partial

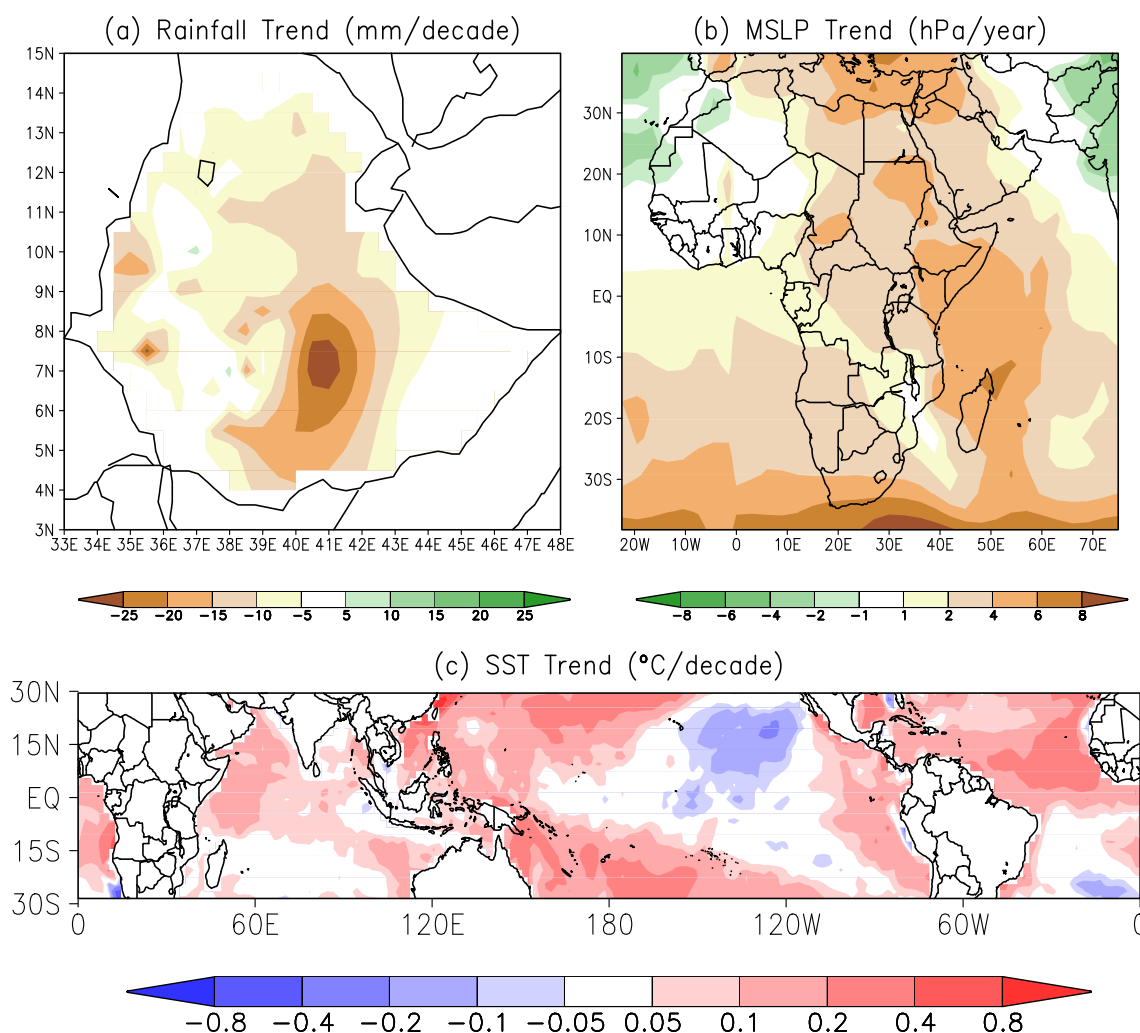


Fig. 3 The linear trend in **a** rainfall, **b** MSLP, and **c** SST over Ethiopia computed from reconstructed FMAM secular variation

Granger causality is applied to the multivariate consisting of spring rainfall over Ethiopia, MSLP pressure over Africa and the spatially averaged secular SSTA representing the northwestern Indian Ocean, southern Indian Ocean, equatorial Atlantic Ocean, northern Pacific Ocean and southern Pacific Ocean basins (see Table 1). The causality analysis reveals that the secular spring rainfall anomaly is forced by only the northwestern Indian Ocean secular SSTA. The causal link is statistically significant at 99 % level. Moreover, the northwestern Indian Ocean secular SSTA forces also the secular MSLP anomaly over parts of Africa indicated in Table 1).

Association of cold/warm secular SST anomaly over Pacific (100–170° W) with easterly/westerly upper level horizontal wind anomalies is observed during spring. However, as the proportion of SST variance from the Pacific ENSO region is negligible (see Fig. 2c), it is likely this association plays some role on secular time scale indirectly by modulating SST in the southeastern Indian Ocean. This is

consistent with the absence of Granger causality between SST from the basin and spring rainfall. On the other hand, large SST variance and warm trend over the northern and southern Pacific (Fig. 2c) might be linked with the large scale upper level atmospheric circulation (e.g., Okoola 2007

Table 1 The latitude-longitude box included in the spatial averaging of secular anomalies of rainfall, MSLP and SST

Variable	Latitude	Longitude
Rainfall	39.0–48° E	3.0–9.0° N
MSLP	20.0–40.0° E	20.0° S–5.0° N
Northwestern Indian SSTA	37.0–75.0° E	15.0° S–30° N
Southern Indian Ocean SSTA	33.0–60.0° E	15.0° S–30° S
Equatorial Atlantic Ocean SSTA	10°–55° W	5.0° S–5.0° N
Northern Pacific Ocean SSTA	150.0° W–120° E	5–30° N
Southern Pacific Ocean SSTA	150.0° W–120° E	5–30° S

and references therein) but does not drive spring rainfall as there is no causal link between the two.

Moreover, our finding that shows an abrupt decline in the southern and southeastern Ethiopia FMAM rains is in agreement with recent results for East African long rains based on observations and three GCMs forced by observed SST to explain the recent decadal drought in the region (Lyon and DeWitt 2012).

The SST forcing affect the atmosphere through hydrostatic and thermodynamic changes of the atmosphere. Therefore, it is important to investigate the dynamical response of the atmosphere to the forcing (e.g., how the dynamical variables such as geopotential heights and wind fields evolve concurrently with rainfall not only at surface but also at low and upper troposphere). For this, MTM-SVD is used to extract joint spatio-temporal secular variation of rainfall, geopotential heights and horizontal winds at 850 and 200 hPa pressure levels over the spatial domain that covers 25° W–75° E and 40° S–40° N. This domain covers areas where dominant large scale circulations that modulate Ethiopian rainfall operate.

5.3 Observed physical mechanisms

The drying trend in rainfall (Fig. 3) is observed over south and southeastern (south of 9° N and east of 38° E) Ethiopia concurrent with SST warming trend over the northwestern Indian Ocean SSTA. Moreover, buildup of pressure over Africa is forced by the northwestern Indian Ocean secular SSTA. This causal link is also apparent in the rise of geopotential height at 850 hPa pressure level (Fig. 4a) over Africa relative to geopotential height over the warm western Indian Ocean and Arabian Peninsula. The atmospheric response

to warm secular SSTA over the northwestern Indian Ocean resulted in wind trends at 850 hPa that exhibit cyclonic flow between the equator and Madagascar over the western Indian Ocean. This cyclonic flow mirrors slightly weaker cyclonic flow in the northern hemisphere with approximate center over the Arabian Sea. Similar cyclonic flows mirror each other with centers over western Africa (near 16° N) and the Atlantic ocean (at around 18° S) along 15° W. The implication of these flows, in response to the high pressure over the continent relative to the low pressure over the Indian Ocean, is the decrease in moisture supply to southern Ethiopia. Specifically, the secular anomalous circulation over the region weakened northeasterly moisture flow from the Arabian Sea into Ethiopia. The Arabian Sea is a major moisture source during this season.

The southwesterly anomaly over the Arabian Sea are related to drying trend over Ethiopia by suppressing the moisture influx from the Indian Ocean (see Fig. 4a). The meridional component of the ITCZ has also weakened as pressure builds up over secular time scale. This condition is associated with weakening of westerlies across the Gulf of Guinea from the Atlantic and Congo Basin (Fig. 4a) due to elevated secular geopotential height anomalies over the central Africa region. The weakening of westerlies has reduced moisture transport from the Atlantic and Congo basins into at least the equatorial Africa. The observed circulation and SST trends can be explained better if we put them in the context of the mean climate during this season. Wet conditions during FMAM prevail provided that a low-level moisture influx toward Ethiopia by strong northeasterly flow on the southeastern margin of the Arabian Sea is high (Camberlin and Philippon 2002b). This condition is clearly absent as the trend in secular geopotential height is

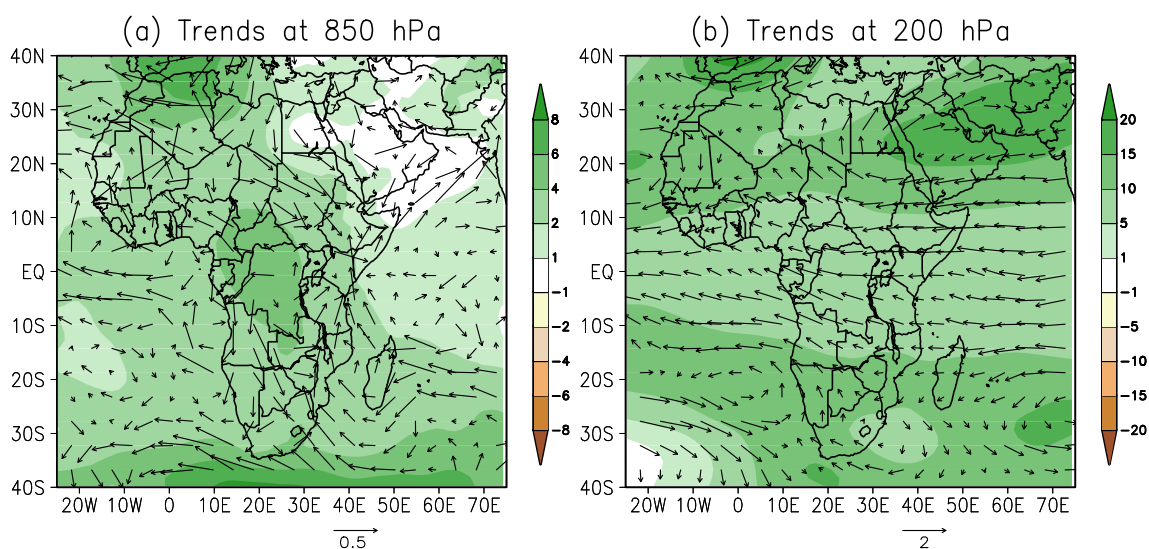


Fig. 4 The linear trend in geopotential heights ($(m^2/s^2)/decade$) and wind anomalies ($(m/s)/year$) at **a** 850 hPa and **b** 200 hPa pressure levels during FMAM

either near normal or negative which resulted in wind trends with weak cyclonic flow. The development of the cyclonic residual circulation over secular time scale weakens the climatological Arabian Sea high (Fig. 4a). As a result the northeasterly flow is also weakened suppressing moisture influx. Because of geopotential height rise/pressure buildup on the secular time scale (Fig. 4a), the intertropical convergence zone (ITCZ) is suppressed both over the continent and western Indian Ocean which served as the zone of surface confluence over Horn of Africa between climatological northeasterly and south-southwesterly winds. In fact, the east-west pressure dipole (high over continent and low over western Indian Ocean) required for wet condition over Horn of Africa (Camberlin and Philippon 2002b) is also enforced by the trend in geopotential heights. However, the secular dipole (Fig. 4a) extends to North Africa and the Arabian Peninsula reducing the strength of climatological dipole (with high pressure over Arabian Peninsula and low pressure over North and West Africa). This trend favors a southward shift of the ITCZ over the western Indian Ocean leading to dry conditions over Horn of Africa. The horizontal wind trend exhibits rather weak southerly component through the Mozambique Channel and along much of the southern half of East African coast (Fig. 4a). The anomalous secular cyclonic flow over Madagascar brings warm air from northern Indian Ocean on its eastern flank and redirects it towards the Mozambique Channel on its western flank. This dilutes a burst of cool air from the southern Indian Ocean thereby hindering initiation of atmospheric instability that is often responsible for convective instability of the second kind during the wet rainfall conditions over East Africa (Okoola, 1999 and references therein).

In the upper troposphere, an anomalous ridge-trough pattern extends from western Europe to the Arabian peninsula during normal to wet FMAM seasons. Specifically, an anticyclonic (warm) feature is found over the central Mediterranean, whereas a cyclonic trough (cold) is located over the Red Sea. Hastenrath (2007) argued that the positive specific humidity anomalies found at 500 hPa on the south-eastern edge of the Red Sea trough as evidence for large-scale convection triggered by strong divergence ahead of the cyclonic curvature or trough extended from the cyclonic flow. However, the upper troposphere (the 200 hPa) zonal winds reveal a predominantly easterly secular anomaly pattern. This is not to be expected if increased divergence is operating as driven by strong local Walker circulation cell. Moreover, this climatological flow at 200 hPa level has been weakening due to positive trend in geopotential height and corresponding anticyclonic flow over Arabian Peninsula on secular time scale. This contributes also to the development of residual cyclonic flow over central Mediterranean (Fig. 4b). The residual cyclonic flow that has evolved over years is in contrast to the anomalous southerly

extension of the subtropical westerly jet over northeast Africa-southwestern Asia, and to weakened westerlies near 30° N at times of wet FMAM conditions reported by Camberlin and Philippon (2002b). In other words, the upper air Subtropical Westerly Jet (STWJ) is weakened by secular anomalous easterly flow at 200 hPa level over Ethiopia and regions south of 20° N. Therefore, the impact is clearly to suppress these flows which are favorable for wet conditions during the season as seen in the observed secular easterly wind anomaly over most of the tropical latitudes (Fig. 4b).

A more recent study by Tierney et al. (2013) has used SST in millennium-long control simulations conducted with fully coupled, atmosphere-ocean general circulation models (CCSM4 of the US National Center for Atmospheric Research (NCAR) and GFDL CM2.1 the Geophysical Fluid Dynamics Laboratory (GFDL) AOGCMs) to show the relationship between annual precipitation in eastern most Africa and SST at multidecadal and longer time scales. The authors have indicated that wet conditions in East Africa are associated with a reorganization of the Walker circulation throughout the tropics, with anomalous rising motion over the central and eastern equatorial Pacific, descending motion over the far western Pacific and eastern Indian Ocean, and another cell of anomalous rising motion over the western Indian Ocean and East Africa for the unfiltered data. These associations are ascribed to typical ENSO features and are consistent with patterns of low-level wind anomalies driven by the SST gradients and associated atmospheric heating anomalies. In contrast, using low-pass-filtered vertical velocity correlations, Tierney et al. (2013) have concluded that the influence of tropical Pacific is considerably weaker on multidecadal and longer timescales. Instead, East African precipitation anomalies are controlled by a Walker circulation anomaly that is localized over the Indian Ocean, with wet conditions associated with ascending motion over East Africa and the western Indian Ocean and descending motion over the eastern Indian Ocean. This holds true over southern and southeastern Ethiopia during wet anomaly periods. However, on the secular time scale as revealed in this study, this mechanism seems to operate but shifted the cell of anomalous rising motion from Eastern Africa into the western Indian Ocean.

5.4 Diagnosis of observed physical mechanisms

Before the use the AGCM model for diagnostic of the observed mechanisms of secular rainfall variability, it is important to verify the model skill in reproducing the observations. Figure 5a shows observed gridded gauge rainfall over Ethiopia (color contour) and wind fields at 925 hPa from ERAInterim. Figure 5b shows rainfall and wind fields at 925 hPa from SPEEDY AGCM for qualitative comparison with the observation in Fig. 5a. The AGCM is forced

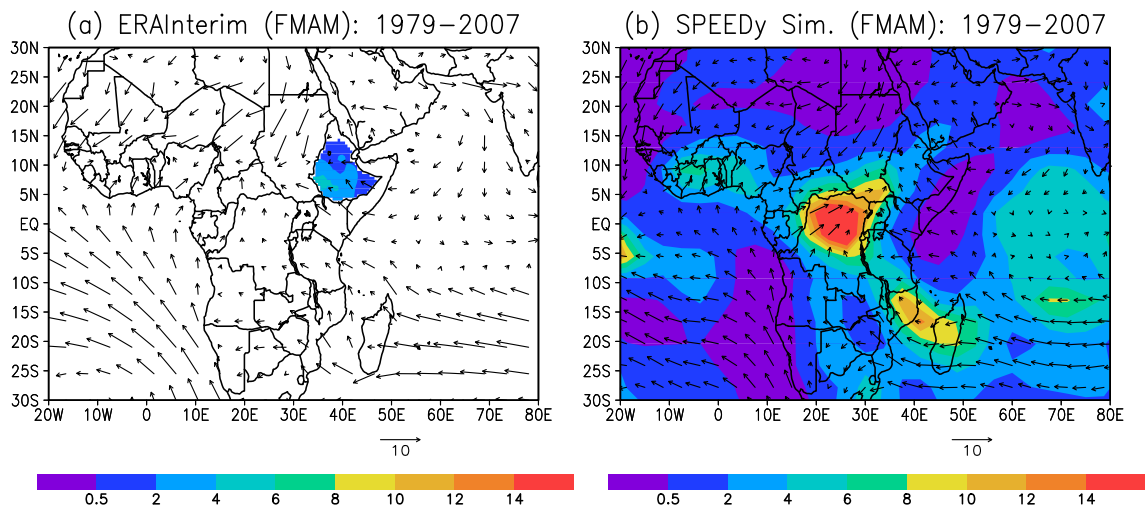


Fig. 5 Observed gauge rainfall (mm/day) and ERAInterim wind fields (m/s) at 925 hPa level (a) and corresponding rainfall (mm/day) and wind fields (m/s) from SPEEDY AGCM averaged for FMAM season over the 1979–2007 period (b)

by observed SST anomaly and coupled to the mixed layer oceanic model in this experiment. The model has reproduced the observed spatial pattern of spring rainfall over Ethiopia while there is a minor difference in the magnitude. For example, climatology of observed rainfall shows that regions south of 10° N and west of 43° E receive spring rainfall (Fig. 5a) which also holds true as seen in the AGCM simulation (Fig. 5b). Moreover, southwestern parts of this area receive more rainfall than the rest in both the AGCM simulation and observation. It is important to note that the model is the simplified SPEEDY AGCM which is not expected to be highly accurate in reproducing the correct magnitude of climate variables, in particular rainfall. Rainfall is a problematic even for more complex and advanced AGCMs/fully coupled AOGCMs.

The atmospheric flows represented by the overlying wind vectors (Fig. 5) show very good agreement between ERAInterim reanalysis and SPEEDY simulation. The easterly and southeasterly flows around the northern flanks of the semipermanent Mascarene and St. Helena high pressure systems respectively are nearly identical in both SPEEDY and ERAInterim. However, there is a minor difference in the wind speeds. Farther north, the northeasterly flows over western Indian Ocean and Arabian Sea in ERAInterim reanalysis (Fig. 5a), which are responsible for major moisture incursion into Ethiopia during spring, are well captured by SPEEDY model (Fig. 5b). The southward shift of ITCZ towards the west coast of Africa and central Africa from its summer position is clearly captured by the wind confluence and the belt of rainfall maximum in the SPEEDY AGCM as good as in the ERA-Interim. Therefore, the model skill is very good and the model can serve not only for sensitivity experiments directed towards understanding the circulation

mechanisms but also can be used in simulating observations despite its simplified nature compared to fully coupled models.

In the following, further assessment of the plausible mechanisms of relating the SST forcing and the atmospheric response as inferred from analysis of observations is made using controlled simulations from AGCM coupled to mixed layer oceanic model as described in Section 4. Although, the secular SST over most Ocean basins have contemporaneous association with spring rain over Ethiopia (see Section 5.1), the Indian Ocean SST is the only one found to have causal link with spring rainfall over Ethiopia and MSLP over Africa as determined by Granger causality analysis. This connection between Indian Ocean SSTA and rainfall over East Africa at secular time scale is quite new, but evidences that connect anomalous Indian Ocean SST to East African multidecadal rainfall variability and the anomalous December–January 1997/98 rainfall exist. The later has been investigated by means of atmospheric model response experiments (Latif et al. 1999). In this study, similar approaches are followed to complement the analysis of observations using the SPEEDY AGCM. The AGCM experiments are designed such that the control experiment is forced by climatological SST everywhere and the sensitivity experiment is forced by climatological SST superimposed on secular SST anomaly over Indian Ocean basin. The sensitivity experiment is the same as control experiment over the rest of the Ocean basins.

Figure 6 shows sensitivity minus control runs averaged over the 1979–2007 period. Figure 6 (left panel) shows rainfall anomaly (color contour) and wind anomaly (vectors) at 850 hPa level. Since the difference between the two simulations is the secular SST anomaly over the Indian Ocean

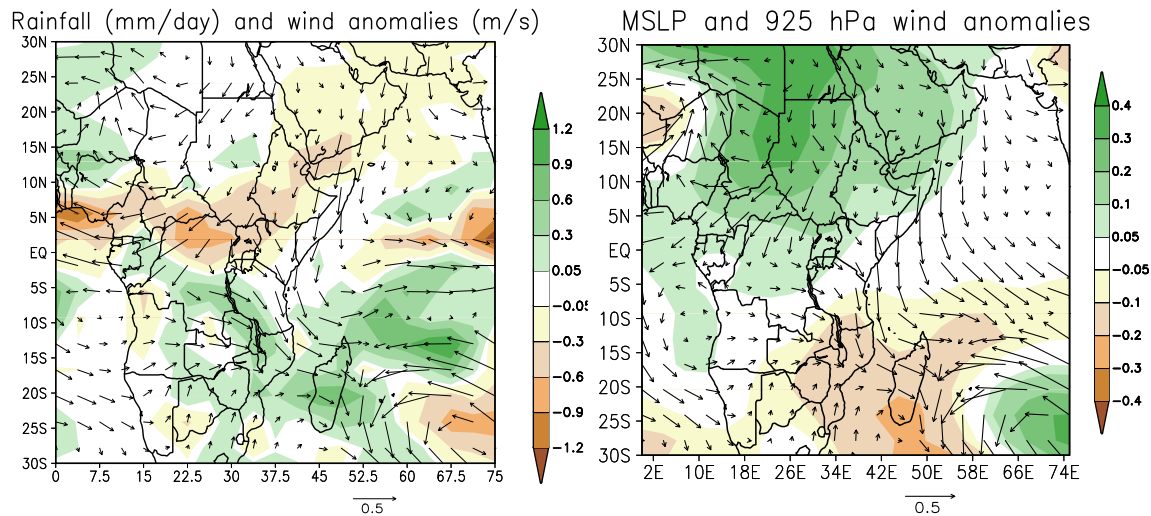


Fig. 6 Response to tropical northwestern Indian Ocean secular SST anomaly (Exp-Ctrl): (Left) Rainfall (color) and 925 hPa wind (vector); (Right) MSLP (color in hPa) and 925 hPa wind (vector in unit of m/s) during FMAM

(see Table 1), the dry secular anomalies over Horn of Africa and equatorial Africa are forced by the Indian Ocean secular SST anomaly. The atmospheric response to the Oceanic forcing is also apparent in the northerly wind anomalies over Horn of Africa, easterly to northeasterly over equatorial Africa west of 30° E and northerly to northwesterly over the western Indian Ocean at 850 hPa. The rainfall anomaly is very much consistent with observed drying as a result of the Indian Ocean warming. The wind anomalies both over the continent and Indian Ocean reflect shift of the low-level wind confluence zone or (ITCZ) southward in response to the warm SST anomalies over the Indian Ocean.

The response to oceanic forcing by the atmosphere led to the buildup of MSLP over much of Africa except southern Africa regions and decrease over the Indian Ocean and western Asia (Fig. 6 (right panel)). This response resembles very much the observed increasing MSLP trend over north Africa and central Africa. The direction of the response agrees also with the observed decreasing trend in MSLP over western Indian Ocean (Fig. 4a).

Two other sets of experiments, that differ from the above two simulations by absence of coupling of the atmosphere to the mixed layer oceanic model, were conducted in order to assess whether prescribed SST is enough to reproduce observed response to secular SST anomalies or not. The results (not shown) reveal that uncoupled simulations could not reproduce the observed secular changes with the same accuracy as coupled simulations. This signifies that Ocean response to atmospheric wind stress by amplifying SST perturbation (positive feedbacks) has significant contribution to the forcing of the rainfall and circulation anomalies. The winds, by causing variations in the depth of the thermocline, can expose cold water to the surface. One of these feedbacks

is the wind-thermocline-SST feedback (commonly known as Bjerknes feedback). The wind-evaporation-SST feedback is another positive feedback that have possibly amplified the SST anomaly. The inadequacy of the uncoupled simulations is in sharp contrast to the commonly taken premise that a reasonable estimate of the SST-forced component of the observed atmospheric circulation is given by AGCM forced with the observed SST. This has been noted for other simulations in the past that find different SST-forced responses from the observed (Kumar et al. 2005; Copsey et al. 2006; Meng et al. 2012). These studies suggest that this premise is inherently flawed. Therefore, the results presented here are based on the coupled simulations.

Figure 7a shows the geopotential and wind anomalies (experiment minus control simulation) at 850 hPa. The rise in geopotential height over slightly expanded region over Africa and Atlantic Ocean in comparison to MSLP buildup as well as drop over southern Africa and Indian Ocean including western Asia reveals the model is robust and able to reproduce the observed anomalies consistently throughout the lower atmosphere. At upper troposphere, the response to the SST forcing reveals that easterly anomalies dominate region between 15° S- 25° N over Africa which weakens the climatological westerly on the southern margin of STWJ. Cyclonic anomalous flow over the western Indian Ocean and part of the East Africa coast indicates subsidence or reduced horizontal outflow at 200 hPa level (Fig. 7b).

The drying trend over Ethiopia (Fig. 3a) including East Africa (not shown) forced by secular SST anomaly is enhanced through feedback generated in response to atmospheric forcing. At lower (850 hPa) and upper troposphere (200 hPa) levels, the rise and drop in geopotential height anomaly as well as accompanying circulation anomalies are

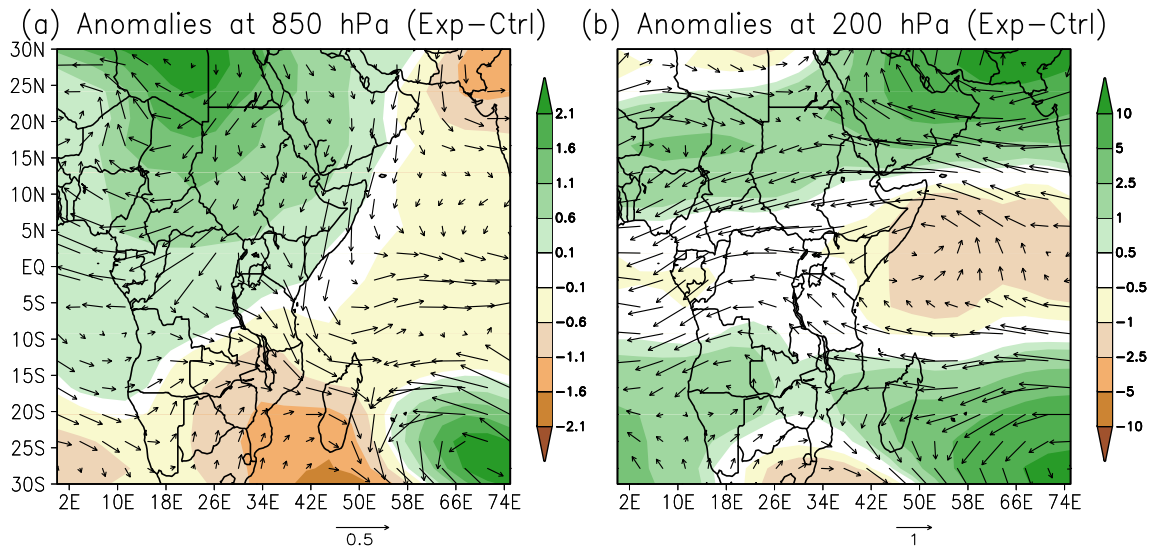


Fig. 7 Response to tropical northwestern Indian Ocean secular SST anomaly (Exp-Ctrl). **a** Geopotential height (color in units of m^2/s^2) and wind anomalies (vector in units of m/s) at 850 hPa. **b** Geopotential

(color) and wind anomalies (vector) at 200 hPa during FMAM in the same units as in (a)

consistently favors dry conditions over the region. Velocity potential anomalies (difference of sensitivity from control simulation) provide a good insight into the atmospheric circulation pattern surrounding the anomalous rainfall forced by SSTA (Mistry and Conway, 2003 and references therein). Thus, velocity potential is a strong dynamical tool to diagnosis convergent and divergent flows at these atmospheric levels. Figure 8 depicts velocity potential anomalies with respect to control simulation at 850 hPa (panel a) and 200 hPa (panel b). Negative velocity potential anomaly (divergence) over East Africa and the Arabian Peninsula at 850 hPa (Fig. 8a) is accompanied by positive velocity potential anomaly (convergence) at 200 hPa level with the exception

of some areas close to the coast (Fig. 8b). Positive velocity potential (convergence) at 850 hPa and negative velocity potential (divergence) anomalies at 200 hPa overlain the warm Indian Ocean region with the exception along the coastal regions. The region of maximum positive anomalies at 850 hPa is located over Madagascar and the surrounding Indian Ocean, suggesting that there is increased convergence in this area thereby enhancing convective activity (see Fig. 6). In contrast, the region of maximum negative velocity potential anomaly in conjunction with upper level positive velocity potential anomaly (subsidence) is found on the land where convective activity is suppressed. This localized response over the ocean is mainly consistent with the

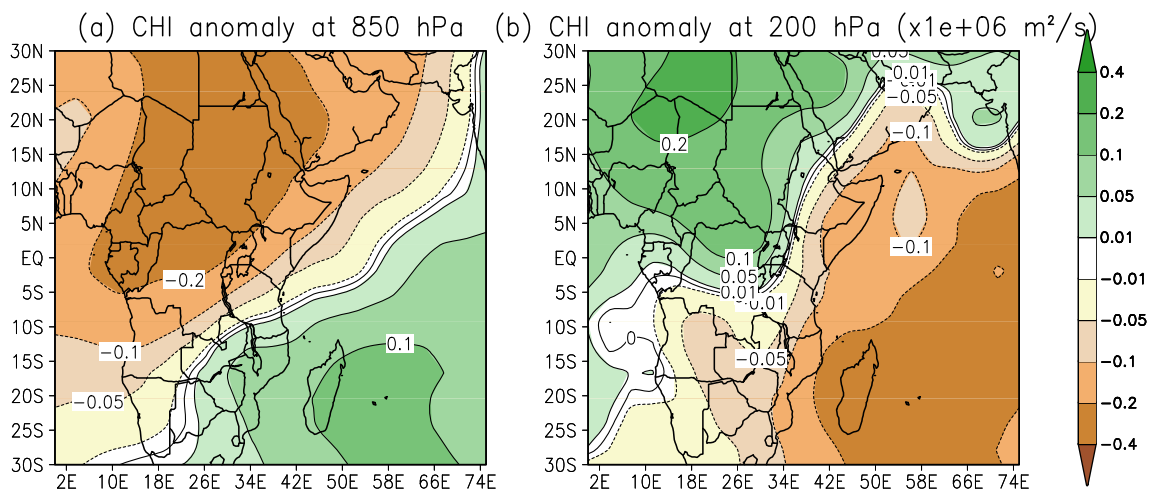


Fig. 8 Response to tropical northwestern Indian Ocean secular SST anomaly (Exp-Ctrl): **a** Velocity potential anomaly (color and contour) at 850 hPa; **b** Velocity potential anomaly (color and contour lines) at

200 hPa during FMAM. Note that the velocity potentials in both panels (a)-(b) are given in units shown at the top of panel (b)

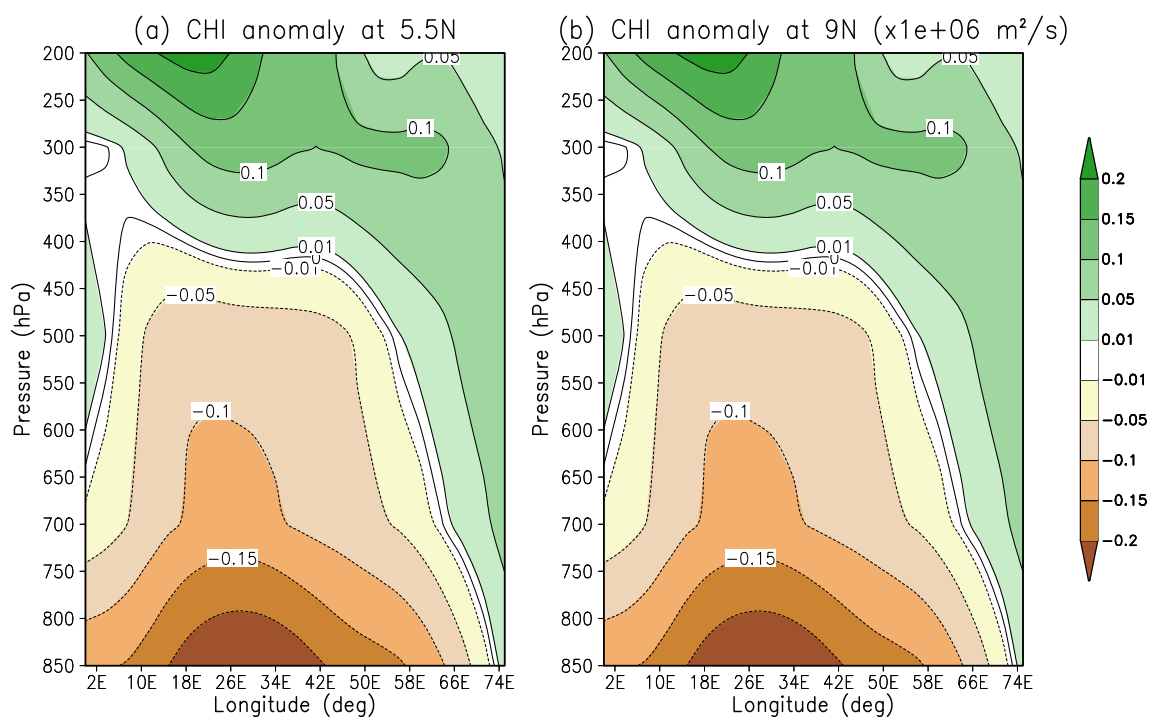


Fig. 9 Longitudinal cross-section of response to tropical northwestern Indian Ocean secular SST anomaly (Exp-Ctrl). **a** Velocity potential anomaly (color and contour) at 5.5° N. **b** Velocity potential anomaly

(color and contour lines) at 9.0° N during FMAM. Note that the velocity potentials in both panels (a)-(b) are given in units shown at the top of panel (b)

fact that the local atmospheric response to the heating is baroclinic whereby warm SST perturbations lead to a low pressure anomaly in the lower troposphere and a high pressure anomaly in the upper (Fig. 7b). The result is also inline with the understanding that the effect of diabatic heating is stronger in the tropics than mid and high latitudes since the atmospheric circulation in tropics is largely modulated by the latent heat released during evaporation from the warm ocean surface.

The longitudinal cross-sections at 5.5° N and 9.0° N show the low-level divergence over Ethiopian latitudes extend into the mid-troposphere (approximately 430 hPa) along 37.5° E (Fig. 9) while the upper level convergence extends from 200 hPa to 400 hPa levels. This deep layer subsidence clearly demonstrates that East Africa has been experiencing atmospheric circulations which reduce rainfall in FMAM in response to secular SST anomaly over Indian Ocean.

While the SPEEDY AGCM, despite its simplicity, has skill to reproduce actual observations if prescribed with observed SST and coupled to the mixed layer ocean model (Kucharski et al. 2009), the above two numerical experiments are not expected to reproduce actual observations. The control experiment can only reproduce climatology whereas the sensitivity experiment aims to see the response of the atmosphere to oceanic forcing on a secular time scale. Since other signals of high frequencies are

not part of the prescribed SST anomalies, the anomaly (sensitivity minus control experiments) in this study enables us to assess the direction of change in the climate variables of interest at the secular time scale. In this case, the main target is rainfall, though it is important to see whether the change in rainfall is physically consistent with atmospheric dynamics (e.g. geopotential height/pressure, wind, velocity potential etc). This has been achieved as the sign of the anomaly and the spatial extent agree very well with observed trends over Ethiopia in particular and East Africa as a whole.

6 Summary and conclusions

The joint coherent spatio-temporal variability of secular rainfall over Ethiopia, MSLP over Africa and adjacent ocean basins and tropical SST is studied. The trend in the secular rainfall anomaly is determined using MK test and Sen's slope estimator. To limit the impact of MK trend test sensitivity to serial correlation, prewhitening is performed. To understand physical mechanisms that led to the observed trend as well as spatio-temporal variability of rainfall over Ethiopia at secular time scale, additional joint MTM-SVD analysis of rainfall, geopotential heights and horizontal winds at 850 and 200 hPa from ECMWF ERA-Interim is performed.

The spring rainfall variance dominates Ethiopian region south of 9° N between 40–43° E and accounts for up to maximum of 50 %. The high fraction of the total variance at secular time scale over this region is indicative of presence of long term changes. These changes may not be necessarily pure slow monotonic trend but may include multidecadal scale variability that can be superimposed on the secular changes due to the limited length of the data. However, such contamination of secular changes can be minimized during the reconstruction by focusing only on the primary mode.

Secular MSLP variance exceeding 60 % of total MSLP variance is seen over Zambia. A small localized variance over Ghana and coastal areas of Gulf of Guinea also contributes to the secular variation. The secular SST variance is maximum over equatorial Atlantic and northwestern India Ocean Basins. High secular SST variance from northwestern India Ocean including Arabian Sea controls spring rainfall over secular time scale.

The linear rainfall trend is downward at all places receiving spring rain with maximum trend exceeding 28 mm.decade⁻¹ over southern highlands. This drying trend might have contributed to the severity of drought events in recent decades over southern Ethiopia. The linear trend derived from secular SST anomaly shows warming over all ocean basins except Pacific region between 100–150°W and small areas near St. Helena high pressure region where dimming trend in secular SST anomaly is observed over the last three decades. However, because of absence causal links between spring rainfall over Ethiopia (as derived from Granger causality analysis) and secular SST over most ocean basins with the exception of Indian Ocean, the role of dimming over the Pacific sub-basin is likely of indirect nature in modulating the long term changes in rainfall.

The buildup of pressure over the Arabian Peninsula and the establishment of the meridional ITCZ arm over central Africa are the major large-scale features during normal to wet spring. However, these systems are weakened by formation of secular anomalous cyclonic and anticyclonic circulation over the Arabian Peninsula and central Africa respectively in the recent decades. Moreover, the important dynamical component of spring rain, STWJ, has been weakened by the establishment of secular easterly anomalies. These secular anomalies in the dynamical fields arise from atmospheric response to SST forcing from northwestern Indian Ocean.

The physical mechanisms, dictating the observed drying trend of Ethiopia in particular and East Africa in general, are determined from secular anomalies extracted using MTM-SVD spectral analysis of observations and reanalysis data sets. The statistical results are also confirmed from atmospheric process studies using physical SPEEDY AGCM. The controlled simulations reveal that Indian Ocean

secular SST anomaly controls spring rainfall trend. As a result, the warming trend over northwestern Indian Ocean causes drying trend over East Africa.

To our knowledge, the findings reported in this study is unique and quantitatively substantiated since the observed rainfall trend is treated along with underlying mechanisms in this way for the first time. These findings clearly have revealed interesting underlying mechanisms that govern the observed secular rainfall variation in the region.

Acknowledgments The author would like acknowledge greatly National Meteorological Services of Ethiopia, ECMWF and BADC for free access to raw gauge rainfall, ERA-Interim and HadSST1 datasets respectively. The author would also like to extend his gratitude to Alexander von Humboldt Foundation for the fellowship as well as the host-Karlsruhe Institute of Technology (KIT) during which this work is completed.

References

- Abdul Aziz O, Burn D (2006) Trends and variability in the hydrological regime of the Mackenzie River Basin. *J Hydrol* 319:282–294
- Adler R, Huffman G, Chang A, Ferraro R, Xie P, Janowiak J, Rudolf B, Schneider U, Curtis S, Bolvin D, Gruber A, Susskind J, Arkin P (2003) The version 2 global precipitation climatology project (GPCP) monthly precipitation analysis (1979–Present). *J Hydrometeor* 4:1147–1167
- Bader J, Latif M (2003) The impact of decadal-scale Indian Ocean sea surface temperature anomalies on Sahelian rainfall and the North Atlantic oscillation. *Geophys Res Lett* 30(22). doi:10.1029/2003GL018,426
- Bahaga TK, Tsidu GM, Kucharski F, Diro G (2014) Potential predictability of the sea-surface temperature forced equatorial East African short rains interannual variability in the 20th century. *QJR Meteorol Soc* p doi:10.1002/qj.2338
- Berrisford P, Dee D, Fielding K, Fuentes M, Kllberg P, Kobayashi S, Uppala S (2009) The ERA-Interim archive Version 1.0 Series: ERA Report Series. ECMWF, Shinfield Park
- Bourke W (1974) A multilevel spectral model. I. Formation and hemispheric integrations. *Mon Weather Rev* 102:687–701
- Bracco A, Kucharski F, Rameshan K, Molteni F (2004) Internal variability, external forcing and climate trends in multi-decadal AGCM ensembles. *Clim Dyn* 23:659–678. doi:10.1007/s00382-004-046-2
- Bracco A, Kucharski F, Molteni F, Hazeleger W, Severijns C (2007) A recipe for simulating the interannual variability of the Asian summer monsoon and its interaction with ENSO. *Clim Dyn* 28:441–460. doi:10.1007/s00382-006-0190-0
- Brubaker KL, Entekhabi A, Eagleson PS (1993) Estimation of continental precipitation recycling. *J Clim* 6:1077–1089
- Camberlin P (1995) June–September rainfall in northeastern Africa and atmospheric signals over the tropics. *Int J Climatol* 15:773–783
- Camberlin P (1997) Rainfall anomalies in the source region of the Nile and their connection with the Indian summer monsoon. *J Climate* 10:1380–1392
- Camberlin P, Philippon N (2002a) The East African March–May rainy season: associated atmospheric dynamics and predictability over the 1968–97 period. *J Climate* 15:1002–1019

- Camberlin P, Philippon N (2002b) The East African March–May rainy season: associated atmospheric dynamics and predictability over the 1968–97 period. *J Climate* 15:1002–1019
- Caminade C, Terray L (2010) Twentieth century Sahel rainfall variability as simulated by the ARPEGE AGCM, and future changes. *Clim Dyn* 35:75–94
- Cannarozzo M, Noto L, Viola F (2006) Spatial distribution of rainfall trends in sicily (1921–2000). *Phys Chem Earth* 31:1921–2000
- Copsey D, Sutton R, Knight JR (2006) Recent trends in sea level pressure in the Indian Ocean region. *Geophys Res Lett* 33:L19,712. doi:[10.1029/2006GL027,175](https://doi.org/10.1029/2006GL027,175)
- Correa-Ramirez MASEH, Morales CE (2012) Spatial patterns of annual and interannual surface chlorophyll-a variability in the Peru-Chile Current System. *Progress Ocenogr* 92–94:8–17
- Dee D, Uppala S, Simmons A, Berrisford P, Poli P, Kobayashi S, Andrae U, Balmaseda M, Balsamo G, Bauer P, Bechtold P, Beljaars A, van de Berg L, Bidlot J, Bormann N, Delsol C, Dragani R, Fuentes M, Geer A, Haimberger L, Healy S, Hersbach H, Holm E, Isaksen L, Kallberg P, Kohler M, Matricardi M, McNally A, Monge-Sanz B, Morcrette JJ, Park B, Peubey C, de Rosnay P, Tavolato C, Thepaut JN, Vitart F (2011) The ERA-Interim reanalysis: configuration and performance of the data assimilation system. *Q J R Meteorol Soc* 137:553–597. doi:[10.1002/qj.828](https://doi.org/10.1002/qj.828)
- Degefu W (1987) Some aspects of meteorological drought in Ethiopia. In: Glantz MH (ed) *Drought and Hunger in Africa*, Montreal. Cambridge University Press, Cambridge
- Delworth TL, Mann ME (2000) Observed and simulated multidecadal variability in the Northern Hemisphere. *Clim Dyn* 16:661–676
- Dinpashoh Y, Jhajharia D, Fakheri-Fard A, Singh VP, Kahya E (2011) Trends in reference crop evapotranspiration over Iran. *J Hydrol* 399:422–433
- Diro GT, Grimes DIF, Black E (2011) Teleconnections between Ethiopian summer rainfall and sea surface temperature: Part I-observation and modelling. *Clim Dyn* 37(1–2):101–119. doi:[10.1007/s00382-010-0837-8](https://doi.org/10.1007/s00382-010-0837-8)
- Elsner JB (2007) Granger causality and Atlantic hurricanes. *Tellus* 59A:476–485
- Folland C, Palmer T, Parker DE (1986) Sahel rainfall and worldwide Sea temperatures. *Nature* 1901–85:320:602–607
- Frankignoul C, Sennechal N (2007) Observed influence of North Pacific SST anomalies on the atmospheric circulation. *J Clim* 20:592–606
- Funk C, Peterson P, Landsfeld M, Pedreros D, Verdin JP, Rowland J, Romero B, Husak G, Michaelsen J, Verdin A (2014) A quasi-global precipitation time series for drought monitoring., vol 832. U.S. Geological Survey Data Series
- Ghil M, Taricco C (1997). In: Castagnoli GC, Provenzale A (eds) *Advanced spectral analysis methods*. Springer, Dresden, pp 137–159
- Ghil M, Allen MR, Dettinger MD, Ide K, Kondrashov D, Mann ME, Robertson AW, Saunders A, Tian Y, Varadi F, Yiou P (2002) Advanced spectral methods for climatic time series. *Rev Geophys* 41:1–41
- Giannini A, Saravanan R, Chang P (2003) Oceanic forcing of Sahel rainfall on interannual to interdecadal time scales. *Science* 302:1027–1030
- Gissila T, Black E, Grimes DIF, Slingo JM (2004) Seasonal forecasting of the Ethiopian summer rains. *Int J Climatol* 24:1345–1358
- Goddard LNEG (1999) Importance of the Indian Ocean for simulating rainfall anomalies over eastern and southern Africa. *J Geophys Res* 104(D16):19,099–19,116
- Granger CW (1969) Investigating causal relations by econometric models and crossspectral methods. *Econometrica* 37(3):424–438
- Guo R, Wang X, Ouyang Z, Li YN (2006) Spatial and temporal relationships between precipitation and ANPP of four types of grasslands in Northern China. *J Environ Sci* 18(5):1024–1030
- Habtemichael A, Pedgley DE (1974) Synoptic case-study of spring rains in Eritrea. *Arch Meteor Geophys Bioklimatol* 34:285–296
- Hagos SM, Cook KH (2008) Ocean warming and late-twentieth-century Sahel drought and recovery. *J Clim* 21:3797–3814
- Hastenrath S (2007) Circulation mechanisms of climate anomalies in East Africa and the equatorial Indian Ocean. *Dyn Atmos Oceans* 43:25–35
- Hastenrath S, Polzin D, Mutai C (2010) Circulation mechanisms of Kenya rainfall anomalies. *J Climate* 24. doi:[10.1175/2010JCLI3599.1:404-4012](https://doi.org/10.1175/2010JCLI3599.1:404-4012)
- Hoerling M, Hurrell J, Eischeid J, Phillips A (2006) Detection and attribution of twentieth-century Northern and Southern African rainfall change. *J Clim* 19:3989–4008
- Jhajharia D, Dinpashoh Y, Kahya E, Singh VP, Fakheri-Fard A (2011) Trends in reference evapotranspiration in the humid region of northeast India. *Hydrol Process* doi:[10.1002/hyp.8140](https://doi.org/10.1002/hyp.8140)
- Jury M (2009) Ethiopian decadal climate variability. *Theor Appl Climatol*
- Kendall M (1975) Rank correlation methods. Charles Griffin, London
- Kucharski F, Molteni F, Bracco A (2006a) Decadal interactions between the western tropical Pacific and the North Atlantic Oscillations. *Clim Dyn* 26:79–91. doi:[10.1007/s00382-005-0085-5](https://doi.org/10.1007/s00382-005-0085-5)
- Kucharski F, Molteni F, Yoo J (2006b) Sst forcing of decadal Indian Monsoon rainfall variability. *Geophys Res Lett* 33:L03,709. doi:[10.1029/2005GL025,371](https://doi.org/10.1029/2005GL025,371)
- Kucharski F, Bracco A, Yoo J, Molteni F (2007) Low-frequency variability of the Indian monsoon-ENSO relationship and the tropical Atlantic: the “weakening” of the 1980s and 1990s. *J Climate* 20:4255–4266
- Kucharski F, Bracco A, Yoo J, Tomkins AM, Feudale L, Ruti P, Aquilla AD (2009) A Gill-Matsuno-type mechanism explains the tropical Atlantic influence on Africa and Indian monsoon rainfall. *Quart J Roy Meteor Soc* 135:569–579. doi:[10.1002/qj.406](https://doi.org/10.1002/qj.406)
- Kumar K, Hoerling M, Rajagopalan B (2005) Advancing dynamical prediction of Indian monsoon rainfall. *Geophys Res Lett* 32:L08,704. doi:[10.1029/2004GL021,979](https://doi.org/10.1029/2004GL021,979)
- Kumar S, Merwade V, Kam J, Thurner K (2009) Streamflow trends in Indiana: effects of long term persistence, precipitation and subsurface drains. *J Hydrol* 374:171–183
- Lamb PJ (1978a) Large-scale tropical Atlantic surface circulation patterns associated with Sub-saharan weather anomalies. *Month Weather Rev Tellus* 30:240–251
- Latif M, Dommengot D, Dima M, Rotzner AG (1999) The role of Indian Ocean sea surface temperature in forcing East African rainfall anomalies during December–January 1997/98. *J Clim* 12:3497–3504
- Lu J (2009) The dynamics of the Indian Ocean sea surface temperature forcing of Sahel drought. *Clim Dyn* 33:445–460
- Lyon B, DeWitt D (2012) A recent and abrupt decline in the East African long rains. *Geophys Res Lett* 39:L02,702
- Mann H (1997) Non parametric tests against trend. *Econometrica* 13:245–259
- Mann ME, Park J (1996a) Joint spatiotemporal modes of surface temperature and sea level pressure variability in the Northern Hemisphere during the Last Century. *J Clim* 9:2137–2162
- Mann ME, Park J (1996b) Greenhouse warming and changes in the seasonal cycle of temperature: model versus observations. *Geophys Res Lett* 23(10):1111–1114
- Mann ME, Lall U, Saltzman B (1995) Decadal-to- centennial-scale climate variability: insights into the rise and fall of the Great Salt Lake. *J Geophys Res* 22(8):937–940

- Meng Q, Latif M, Park W, Keenlyside NS, Semenov VA, Martin T (2012) Twentieth century Walker circulation change: data analysis and model experiments. *Clim Dyn* 38:1757–1773
- Mengistu Tsidu G (2012) High-resolution monthly rainfall database for Ethiopia: homogenization, reconstruction, and gridding. *J Clim* 25:8422–8443
- Mengistu Tsidu G, Ture K (2013) Mechanisms of ozone enhancement during stratospheric intrusion coupled with convection over upper troposphere equatorial Africa. *Atmos Environ* 70:410–424. doi:[10.1016/j.atmosenv.2013.01.024](https://doi.org/10.1016/j.atmosenv.2013.01.024)
- Mengistu Tsidu G, Ture K, Sivakumar V (2013) Observational evidence of planetary wave influences on ozone enhancements over upper troposphere North Africa. *Atmospheric Research* 129:130:1–19. doi:[10.1016/j.atmosres.2013.04.001](https://doi.org/10.1016/j.atmosres.2013.04.001)
- Mengistu Tsidu G, Blumenstock T, Hase F (2015) Observations of precipitable water vapour over complex topography of Ethiopia from ground-based GPS, FTIR, radiosonde and ERA-Interim reanalysis. *Atmos Meas Tech* 8:3277–3295. doi:[10.5194/amt-8-3277-2015](https://doi.org/10.5194/amt-8-3277-2015)
- Mistry VV, Conway D (2003) Remote forcing of east African rainfall and relationships with fluctuations in levels of Lake Victoria. *Int J Climatol* 23:67–89
- Mitchell T, Jones P (2005) An improved method of constructing a database of monthly climate observations and associated high-resolution grids. *Int J Climatol* 25:693–712. doi:[10.1002/joc.1181](https://doi.org/10.1002/joc.1181)
- Molten F (2003) Atmospheric simulations using a GCM with simplified physical parameterizations. I. Model climatology and variability in multi-decadal experiment. *Clim Dyn* 20:175–191
- Mutai CC, Ward MN (2000) East African rainfall and the tropical circulation/convection on intraseasonal to interannual time scales. *J Clim* 13:3915–3939
- Mwale D, Gan TY (2005) Wavelet analysis of variability, teleconnectivity, and predictability of the September–November East African rainfall. *J Appl Meteorol* 44:256–269
- Nicholson SE, Grist JP (2003) The seasonal evolution of the atmospheric circulation over West Africa and equatorial Africa. *Clim Dyn* 16(7):1013–1030
- Nickolson SE (1996) A review of climate dynamics and climate variability in Eastern Africa. In: Johnson TC, Odada EO (eds) *The liminology, climatology and paleoclimatology the East African Lakes*. Gordon and Breach Publishers, pp 25–56
- Ogallo LJ (1989) The spatial and temporal patterns of the East African seasonal rainfall derived from principal component analysis. *J Climatol* 9:145–167
- Oguntunde P, Friesen J, van de Giesen N, Savenije H (2006) Hydroclimatology of volta River Basin in West Africa: trends and variability from 1901 to 2002. *Phys Chem Earth* 31:1180–1188
- Okoola R (1999) A diagnostic study of the eastern Africa monsoon circulation during the Northern Hemisphere spring season. *Int J Climatol* 19:143–168
- Oppo DW, Rosenthal Y, Linsley BK (2009) 2,000-year-long temperature and hydrology reconstructions from the Indo-Pacific warm pool. *Nature* 460:1113–1116
- Rayner NA, Parker DE, Horton EB, Folland CK, Alexander LV, Rowell DP, Kent EC, Kaplan A (2003) Global analyses of sea surface temperature, sea ice, and night marine air temperature since the late nineteenth century. *J Geophys Res* 108(D14):4407. doi:[10.1029/2002JD002,670](https://doi.org/10.1029/2002JD002,670)
- Schreck C, Semazzi F (2004) Variability of the recent climate of Eastern Africa. *Int J Climatol* 24:681–701
- Segele Z, Lamb P (2005) Characterization and variability of Kiremt rainy season over Ethiopia. *Meteorology and Atmospheric Physics* 89:153–180
- Segele Z, Leslie L, Lamb P (2008) Evaluation and adaptation of a regional climate model for the Horn of Africa: rainfall climatology and interannual variability. *Inter J Climatol*
- Seleshi Y, Camberlin P (2006) Recent changes in dry spell and extreme rainfall events in Ethiopia. *Theor Appl Climatol* 83:181–191
- Seleshi Y, Demaree G (1995) Rainfall variability in the Ethiopian and Eritrean highlands and its links with the Southern Oscillation. *J Biogeograph* 22:945–952
- Seleshi Y, Zanke U (2004) Recent changes in rainfall and rainy days in Ethiopia. *Int J Climatol* 24:973–983
- Shanku D, Camberlin P (2005) The effect of the southwest Indian Ocean tropical cyclones on Ethiopian drought. *Int J Climatol* 18:1373–1378
- Slingo J, Spencer H, Hoskins B, Berrisford P, Black E (2005) The meteorology of the western Indian Ocean and the influence of the East African Highlands. *Philos Trans R Soc A* 363:25–42
- Smirnov D, Mokhov II (2009) From Granger causality to long-term causality: application to climatic data. *Phys Rev E* 80. doi:[10.1103/PhysRevE.80.016,208](https://doi.org/10.1103/PhysRevE.80.016,208)
- Smirnov D, Mokhov II (2015) Relating Granger causality to long-term causal effects. *Phys Rev E* 92. doi:[10.1103/PhysRevE.92.042,138](https://doi.org/10.1103/PhysRevE.92.042,138)
- Somkiat Y, McCabe GJ, Rajagopalan B, Gangopadhyay S (2009) Joint spatiotemporal variability of global sea surface temperatures and global palmer drought severity index values. *J Clim* 22:6251–6267
- Sun L, Semazzi F, Giorgi F, Ogallo L (1999b) Application of the NCAR regional climate model to eastern Africa. Part II: simulation of interannual variability of short rains. *J Geophys Res* 104:6549–6562
- Sylla M et al. (2009) Multiyear simulation of the African climate using a regional climate model (RegCM3) with the high resolution ERA-interim reanalysis. *Clim Dyn*
- Tierney JE, Smerdon JE, Anchukaitis KJ, Seager R (2013) Multi-decadal variability in East African hydroclimate controlled by the Indian Ocean. *Nature* 493:389–392
- Trenberth KE, Dai A, Rasmussen RM, Parsons DB (2003) The changing character of precipitation. *Bull Am Meteorol Soc*:84
- Vizy E, Cook K (1998) Connections between the summers East African and Indian rainfall regimes. *J Geophys Res* 103(D16):4510. doi:[10.1029/2003JD003,452](https://doi.org/10.1029/2003JD003,452)
- Wang XL, Chen H, Wu Y, Feng Y, Pu Q (2010) New techniques for detection and adjustment of shifts in daily precipitation data series. *J Appl Meteor Climatol* 49:2416–2436
- Xie P, Arkin PA (1996) Analysis of global monthly precipitation using gauge observations, satellite estimates, and numerical model predictions. *J Clim* 95:840–858
- Xie P, Arkin PA (1997) Global precipitation: a 17-year monthly analysis based on gauge observations, satellite estimates, and numerical model outputs. *Bull Amer Meteor Soc* 78:2539–2558
- Zhou G, Minakawa N, Githeko A, Yan G (2006) Climate variability and malaria epidemics in the highlands of East Africa. *Trends Parasitol* 21:52